

P91 钢焊缝蠕变的非线性超声检测

原可义, 韩赞东, 陈以方, 钟约先

(清华大学 机械工程系先进成型制造教育部重点实验室, 北京 100084)

摘 要: 分析了金属材料蠕变过程中的非线性应力—应变关系, 指出在蠕变超声检测过程中存在非线性波动现象. 讨论了使用脉冲超声实现非线性检测的方法, 即利用超声检测信号高频段与低频段的能量之比作为非线性的表征. 分析了衰减对非线性检测的影响, 并根据频率—衰减关系对非线性参数的计算方法做出了修正. 应用该方法对不同蠕变状态的 P91 钢母材及焊缝热影响区进行了检测. 结果表明, 非线性参数随蠕变时间的增加呈上升趋势; 该方法可以有效区分同一材质的不同蠕变状态, 可以作为 P91 钢焊缝蠕变程度相对性检测的有效方法.

关键词: 耐热钢; 超声; 非线性; 焊缝

中图分类号: TG115.28 **文献标识码:** A **文章编号:** 0253-360X(2013)09-0083-04



原可义

0 序 言

P91 钢是目前主要的高温管道用钢. 管道中存在着大量的焊接结构, 焊缝区域的蠕变性能通常要弱于母材, 因此高温管道常常由于蠕变损伤而导致 IV 类焊缝失效^[1, 2]. 为了准确估算管道的剩余寿命, 保证高温设备的安全和效率, 如何准确评价材料的蠕变状态已经得到越来越多的关注^[3, 4]. 相对于传统的蠕变寿命评价方法^[5, 6], 超声检测方法具有不破坏构件完整性、可在线检测等优点, 因此应用超声检测评价焊接构件的蠕变寿命得到了广泛的研究^[7].

应用超声对蠕变状态的检测不同于对宏观缺陷的检测, 宏观缺陷的尺寸与波长在同一数量级, 可以用反射能量对宏观缺陷进行检测; 蠕变形成的微孔洞及晶界析出物等尺寸通常在微米量级^[8, 9], 由于该尺寸远小于超声波长, 反射能量法对蠕变状态的检测灵敏度很低.

为提高超声对蠕变状态检测的灵敏度, 针对不同的检测对象, 研究者尝试了不同的检测参数^[10, 11], 其中, 非线性超声检测是一种较为新颖的检测方法, 应用非线性超声对金属的蠕变进行检测尚处于试验阶段. 目前的检测试验大多以连续波理论为基础, 使用一定长度的脉冲串激励, 以尽量保证激励信号的单频特性. 而实际超声检测中通常使用

脉冲信号进行激励, 检测信号具有一定频谱宽度, 在此条件下的超声非线性特征更为复杂. 文中讨论了使用通用的超声检测设备, 脉冲激励条件下, 应用超声非线性特征对 P91 钢及其焊缝的蠕变情况进行评价的方法. 此方法利用超声衰减与频率的关系对蠕变引起的声衰减进行修正, 并以“超声非线性体现了能量从低频向高频转移的特性”这一特点为前提, 以超声检测信号高频段与低频段的能量比率为检测参数, 实现了对不同蠕变状态的检测.

文中利用该方法对 P91 钢及其焊缝的蠕变状态进行了评价. 结果表明, 该方法可以区分不同蠕变状态的 P91 钢及其焊缝. 该方法使用的检测参数可以作为金属蠕变非线性超声检测的敏感参数.

1 蠕变非线性超声检测原理

蠕变通常是指金属材料在高于 $0.5T_m$ 温度, 受到低于其屈服应力的载荷时所发生的连续塑性变形过程, 其中 T_m 为对应金属的熔点. 蠕变是一个长时间微缺陷萌生、累积的过程, 经典的金属材料蠕变本构方程可表述为

$$\dot{\varepsilon} = Q\sigma^n \quad (1)$$

式中: $\dot{\varepsilon}$ 为应变张量; σ 为应力张量; Q 和 n 为与材料有关的参数. 将式(1)改写为应力应变关系, 即

$$\sigma = \left(\frac{1}{Qt} \right)^{\frac{1}{n}} (\varepsilon)^{\frac{1}{n}} \quad (2)$$

式中: t 为时间变量; 其它各项与式(1)相同. 由式

(2) 可以看出,蠕变的本构方程为一个非线性的时变方程,其瞬时的应力张量与应变状态和时间有关。由于金属材料的蠕变为一个长时间的缓变过程,其时间单位通常为分钟(min)或小时(h),而超声检测过程相对而言为一个短时过程,其时间单位通常为微秒(μs),因此在一次超声检测过程中可以认为式(2)中的时间参数为不变量;其次,超声检测使用的超声波引起的形变相对于蠕变引起的塑性形变为小量,则针对某一次的超声检测,可以将式(2)进行 Taylor 展开,即

$$\sigma = E \varepsilon \left(1 - \frac{1}{2} \beta \varepsilon + \frac{1}{3} \delta \varepsilon^2 + \dots \right) \quad (3)$$

式中: E 为瞬时的弹性模量; β 为二次非线性系数; δ 为三次非线性系数,其它各项与式(1)相同。忽略式(3)中三次以上的高阶项,则一维波动方程的平面波解为

$$\begin{aligned} u(x, t) = & a_1 \sin(\omega t - kx) + b_1 \frac{x}{h} \cos(\omega t - kx) \\ & + a_2 \frac{x}{h} \cos(2\omega t - 2kx) + a_3 \frac{x}{h} \cos(3\omega t - 3kx) \end{aligned} \quad (4)$$

式中: $u(x, t)$ 为平面波位移; x 为传播方向上的位置变量; t 为时间变量; a_1 为基频正弦幅值; ω 为超声波的基频(圆频率); k 为传播方向上的波数; b_1 为基频余弦幅值系数; h 为传播方向上的介质厚度; a_2 为二次谐频余弦幅值系数; a_3 为三次谐频余弦幅值系数。

式(4)中的各次谐频余弦幅值系数与材料的非线性系数有关,可以表达如下

$$\left. \begin{aligned} b_1 &= \frac{\delta h}{8c^3} a_1^3 \omega^3 \\ a_2 &= \frac{\beta h}{8c^2} a_1^2 \omega^2 \\ a_3 &= \frac{\delta h}{24c^3} a_1^3 \omega^3 \end{aligned} \right\} \quad (5)$$

式中: c 为超声传播方向上的弹性波速度;其它符号与上文相同。

由上述分析可以看出,蠕变增强了材料的非线性特征。当蠕变材料受到超声波激励时,在传播过程中会出现高次谐波,即超声波在材料中传播的过程中,存在着从低频段向高频段的能量转移。当使用单频超声波(频域具有分离谱特征)检测时,可以明确的指出二次谐波和三次谐波的幅度,而对于实际检测中使用的脉冲波(频域具有连续谱特征),由于其存在一定的带宽(图1),无法分离出不同频率对应的高次谐波,只能通过高频段与低频段的能量比率来估算材料的非线性程度。

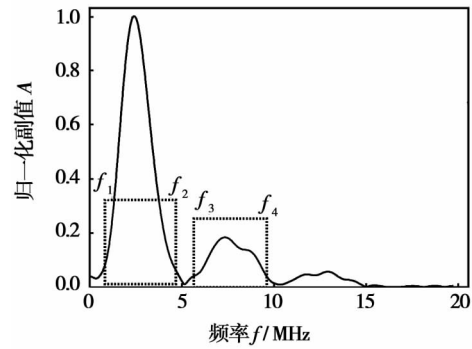


图1 实际检测中脉冲波的频谱

Fig. 1 Frequency spectrum of pulse wave from practical testing

如图1所示,以频率 $f_1 \sim f_2$ 为低频段的门限, $f_3 \sim f_4$ 为高频段的门限,则可使用下式对材料的非线性进行估计,即

$$P_{\text{non}} = \frac{\int_{f_3}^{f_4} A^2(f) df}{\int_{f_1}^{f_2} A^2(f) df} \quad (6)$$

式中: P_{non} 为非线性参数; $A(f)$ 为超声信号的幅度谱; f 为超声信号的频率; $[f_1, f_2]$ 为低频段的积分区间; $[f_3, f_4]$ 为高频段的积分区间。式(6)即为检测信号高频段和低频段的能量比。

上述结果是在忽略声衰减的条件下获得的,由于式(6)涉及到了不同频率的超声能量,而不同频率的超声衰减系数是不同的,因此有必要对不同频率的超声衰减进行修正。通常认为,对于蠕变的金属,超声的衰减系数与对应超声频率的四次方成正比^[12],使用频率的四次方对检测信号的幅度谱进行修正,则式(6)可改写为

$$P_{\text{non}} = \frac{\int_{f_3}^{f_4} (f^4 A(f))^2 df}{\int_{f_1}^{f_2} (f^4 A(f))^2 df} \quad (7)$$

式中变量的定义与式(6)相同。式(7)即为文中所使用的脉冲超声非线性评价参数。

2 检测试验

检测采用穿透法,使用通用的脉冲激励信号源。所用的激励探头中心频率为 2.2 MHz,其频响如图 2a 所示;为保证高频段的接收灵敏度,选用的接收探头中心频率为 11 MHz,频响如图 2b 所示。

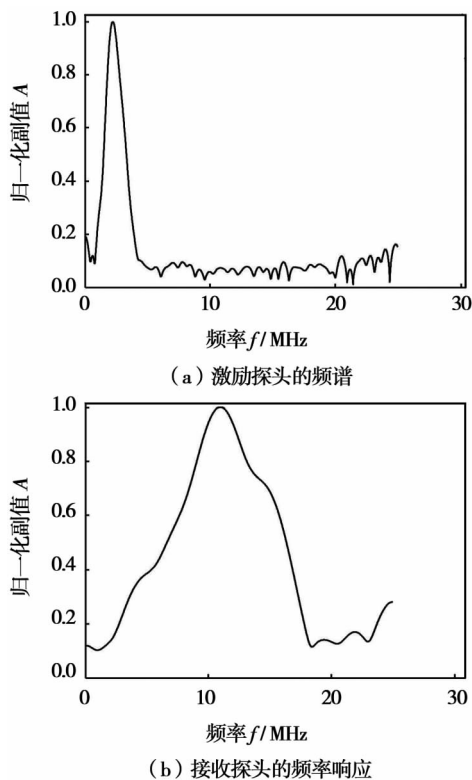


图2 超声检测探头的频率特征

Fig. 2 Frequency characteristics of ultrasonic testing probes

应用式(7)所示的检测参数,分别对蠕变时间为0 h,120 h和250 h的P91钢进行检测,测量结果如表1所示.由表1的数据中可以看出,该参数可以区分出不同蠕变状态的P91钢,但其参数值变化幅度不大,这也反映出P91钢具有较强的高温蠕变抗性.

表1 P91钢蠕变的脉冲超声非线性测量结果

Table 1 Nonlinear pulse ultrasonic testing results of P91 steel creep

蠕变时间 t/h	0	120	250
非线性参数	143.28	153.06	156.03

如前文所述,高温设备的蠕变失效多发生于焊缝位置,因此焊缝为蠕变超声检测的重点位置.P91钢的焊缝结构通常可划分为3部分,即母材区、热影响区和焊缝区.其中,热影响区为母材和焊缝间的过渡结构,是蠕变破坏的危险位置,因此选择的检测点位于热影响区,如图3所示.沿厚度方向上中下位置各取一点作为检测点.图3所示即为超声检测的检测面,超声波平行于焊缝入射,图3中所标检测点即为超声探头的耦合位置,为保证耦合条件,两个检测面均进行了加工.试验使用3个P91钢焊缝蠕变试块作为检测对象,其蠕变时间分别为0 h,120 h和

250 h.

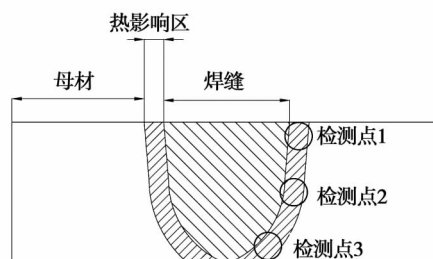


图3 焊缝的基本结构及检测位置

Fig. 3 Basic composition of weldments and inspection position

检测结果如表2所示,可以看出式(7)所示的参数可以区分焊缝热影响区对应位置的不同蠕变状态,并且与表1中的数据呈现相同的上升趋势,即随着蠕变时间的增加,式(7)所示的非线性参数值随之增加.但也应该注意到,母材(表1)与热影响区(表2)的测量绝对值并不一致,母材处的无蠕变参数值大于热影响区处的蠕变参数值,这应该是由材质的区别造成的.这也说明该参数只适用于相对性测量,而不能通过绝对数值对材料的蠕变状态进行表征.

表2 热影响区的脉冲超声非线性测量结果

Table 2 Nonlinear pulse ultrasonic testing results of P91 steel HAZ creep

蠕变时间 t/h	检测位置		
	1	2	3
0	77.48	93.75	91.34
120	117.47	126.09	128.49
250	155.60	143.30	212.45

3 结 论

(1) 提出了一种使用脉冲超声进行非线性超声检测的方法,使用检测信号高频段与低频段的能量比值作为超声非线性的表征参数,并根据衰减与频率的关系对不同频率的幅度谱进行了修正.

(2) 应用该方法对P91钢及其焊缝的蠕变检测试验表明,该参数能够区分同一材质的不同蠕变状态,可以应用于高温材料的蠕变检测.

(3) 该方法在母材位置和焊缝位置测得的绝对值不同,表明该方法受材质的影响较大,只能针对同一材质进行相对性的检测.对于绝对测量方法,还

需要更为深入的研究.

参考文献:

- [1] 孟庆森, 韩培德, 杨世杰, 等. 铁素体 - 奥氏体异种钢接头的界面组织及力学性能[J]. 焊接学报, 1997, 18(2): 26 - 30.
Meng Qingsen, Han Peide, Yang Shijie, *et al.* Interface structure and mechanical property of F/A dissimilar metal welded joints[J]. Transactions of the China Welding Institution, 1997, 18(2): 26 - 30.
- [2] 田志凌, Steen M. X20CrMoV12·1 钢焊接接头的蠕变行为[J]. 焊接学报, 1992, 13(2): 79 - 84.
Tian Zhiling, Steen M. Creep behaviour of X20CrMoV12·1 welded joint[J]. Transactions of the China Welding Institution, 1992, 13(2): 79 - 84.
- [3] Hong Seong-gu, Lee Soon-bok. Mechanism of dynamic strain aging and characterization of its effect on the low-cycle fatigue behavior in type316L stainless steel[J]. Journal of Nuclear Materials, 2005, 340(3): 307 - 314.
- [4] 张国栋, 周昌玉. 焊接残余应力对焊接接头蠕变性能的影响[J]. 焊接学报, 2007, 28(8): 99 - 102.
Zhang Guodong, Zhou Changyu. Effects of welding residual stress on creep of welded joint[J]. Transactions of the China Welding Institution, 2007, 28(8): 99 - 102.
- [5] Lokoshchenko A M. Application of kinetic theory to the analysis of high-temperature creep rupture of metals under complex stress (review) [J]. Journal of Applied Mechanics and Technical Physics, 2012, 53(4): 599 - 610.
- [6] Neubauer B, Wedel U. NDT: Replication avoids unnecessary replacement of power plant components [J]. Power Engineering (Barrington, Illinois), 1984, 88(5): 44 - 47.
- [7] Sposito G, Ward C, Cawley P, *et al.* A review of non-destructive techniques for the detection of creep damage in power plant steels [J]. NDT&E International, 2010, 43(7): 555 - 567.
- [8] Hiroaki Hatanaka, Nobukazu Ido, Takuya Ito, *et al.* Ultrasonic creep damage detection by frequency analysis for boiler piping [J]. Journal of Pressure Vessel Technology, 2007, 129(4): 713 - 718.
- [9] 马 崇, 荆洪阳, 徐连勇, 等. P92 钢 IV 型开裂的显微组织变化[J]. 焊接学报, 2009, 30(8): 49 - 52.
Ma Chong, Jing Hongyang, Xu Lianyong, *et al.* Microstructure investigation on Type IV cracking in P92 steel [J]. Transactions of the China Welding Institution, 2009, 30(8): 49 - 52.
- [10] Maharaj C, Dear J P, Morris A. A Review of methods to estimate creep damage in low-alloy steel power station steam pipes [J]. Strain, 2009, 45(4): 316 - 331.
- [11] Kim Chungseok. Creep damage characterization of Ni-based superalloy by acoustic nonlinearity [J]. Progress in Natural Science-materials International, 2012, 22(4): 303 - 310.
- [12] Gomez Alvarez-Arenas T, Riera-Franco de Sarabia E, Gallego-Juarez J A. Ultrasonic evaluation of creep damage in steel [J]. Ultrasonics, 1993, 31(3): 155 - 159.

作者简介: 原可义, 男, 1982 年出生, 博士研究生. 主要从事无损检测方面的研究. Email: yuankeyi@gmail.com

通讯作者: 韩赞东, 男, 博士, 副教授, 博士研究生导师. Email: hanzd@tsinghua.

Abstract: Numerical simulation of resistance spot welding of high strength DP590 steel and 6061 aluminum alloy was carried out by finite element method (FEM) software SORPAS. Three stages of nugget formation process of steel-aluminum RSW had been analyzed. Meanwhile , the nugget offset phenomenon and dual nugget characteristics caused by asymmetric temperature distribution field feature of steel-aluminum RSW had been elaborated. The macro and micro structure of the weld was examined with EDS , and the dynamic resistance of the welded zone was measured. The results revealed that the melted aluminum alloy spread and diffused on the interface between the steel and aluminum , which led to the formation of fusion-brazed joint. The thickness of intermetallic compound (IMC) is less than 2 μm while the atomic percentage of aluminum diffused in steel are about 40% .

Key words: resistance spot welding; numerical simulation; joint interface; steel-aluminum

Effect of plunge depth on interface distortion in friction stir spot welding

ZHOU Guannan¹ , SHEN Yifu¹ , LI Bo¹ , YAO Lei¹ , WU Xiaowei¹ , HU Weiye² (1. College of Materials Science and Technology , Nanjing University of Aeronautics and Astronautics , Nanjing 210016 , China; 2. Technology Research Institute of Nanjing Chenguang Group Co. , Ltd (NCGC) , China Aerospace Science and Industry Corporation (CASTC) , Nanjing 210012 , China) . pp 75 – 78

Abstract: Base on the copper foil tracer method , the parameters for friction stir spot welding 2mm-thick 6061-T6 aluminum alloy sheet was optimized. The influence of different plunge depths on the characteristic evolution and mechanical properties of joint interface was investigated by setting the geometric characteristic parameters of interface distortion. The experimental results reveal that the effect of plunge depth on the interface distortion morphology was most significant , comparing to other welding parameters. Increasing the plunge depth could almost eliminate the interface warping , increase the width of effective bonded area and shear strength of the joint.

Key words: friction stir spot welding; interface distortion; plunge depth; copper foil tracer

Characteristics of weld formation in variable polarity plasma arc horizontal welding of 2A14 aluminum alloy

ZHANG Qinlian , YANG Chunli , LIN Sanbao , FAN Chenglei (State Key Laboratory of Advanced Welding and Joining , Harbin Institute of Technology , Harbin 150001 , China) . pp 79 – 82

Abstract: The variable polarity plasma arc welding of 6mm thick 2A14 aluminum alloy sheets was carried out. The reason for defects occurred during horizontal welding was clarified through analyzing the forces acting on the welding pool. The difficulties in VPPA horizontal welding were formation of undercuts on both sides and the gathering of blowholes around the boundary in upper part of the weld. It was found that less welding heat input was beneficial for avoiding the undercut on top side , but larger welding heat input was beneficial for reducing undercut on bottom side. The defects during horizontal welding might be at-

tributed to the fluid flow caused by gravity or the balance of the forces acting on the welding pool.

Key words: variable polarity plasma arc(VPPA) ; horizontal welding of aluminum alloy; weld formation; weld defect

Detection of creep damage in P91 steel weldments using nonlinear ultrasonic technique

YUAN Keyi , HAN Zandong , CHEN Yifang , ZHONG Yuexian (Department of Mechanical Engineering , Tsinghua University , Beijing 100084 , China) . pp 83 – 86

Abstract: Nonlinear stress-strain relation in creeping metal was analyzed. The nonlinear fluctuation in creep damage detection with ultrasound was described. A new nonlinear ultrasonic method using pulse wave was proposed , in which the energy ratio of high frequency band to low frequency band of ultrasonic signal was used to characterize the nonlinearity caused by creeping. The influence of attenuation was discussed , and correction to the new nonlinear ultrasonic method was obtained according to frequency-attenuation relation. The base metal and heat-affected zone (HAZ) of P91 steel weldments in different creeping states were detected with this corrected nonlinear ultrasonic method. And the results showed that the nonlinear ultrasonic parameter increased while the creep time increased , and the new method could distinguish different creep states of the same texture. Therefore , this new nonlinear ultrasonic method could be effective for detecting the creep damage degree of P91 steel weldments.

Key words: creep-resistant steel; ultrasonic; nonlinearity; weldment

Thermodynamic analysis of interfacial reaction by pulsed DE-GMAW for aluminum-steel dissimilar metals

SHI Yu¹ , SHAO Ling² , HUANG Jiankang² , GU Yufen² (1. State Key Laboratory of Gansu Advanced Non-Ferrous Metal Materials , Lanzhou University of Technology , Lanzhou 730050 , China; 2. Key Laboratory of Non-Ferrous Metal Alloys , The Ministry of Education , Lanzhou University of Technology , Lanzhou 730050 , China) . pp 87 – 90

Abstract: ER5356 aluminum alloy wire was welded on galvanized steel sheet by pulsed DE-GMAW process. The best weld morphology was obtained by adjusting the welding parameters. The results indicate that fusion-brazing between aluminum alloy and galvanized steel was achieved by pulsed DE-GMAW process. The microstructure of the interface in joint was observed and analyzed with SEM and EDS , and Fe_2Al_5 and FeAl_3 intermetallic compound layers formed in the interface. The Gibbs free energies of Fe_2Al_5 and FeAl_3 intermetallic compounds were calculated with Thermo-Calc software , and it was found that the Gibbs free energy of Fe_2Al_5 was smaller than that of FeAl_3 at high temperature , but the Gibbs free energy of FeAl_3 was smaller than that of Fe_2Al_5 at low temperature. The results show that Fe_2Al_5 intermetallic compound formed first during welding , and subsequently FeAl_3 intermetallic compound formed and precipitated upon cooling.

Key words: pulsed DE-GMAW; aluminum-steel weld-